



**Aerosol  
hygroscopicity  
measurements  
during CARES 2010**

D. B. Atkinson et al.

# Aerosol optical hygroscopicity measurements during the 2010 CARES Campaign

D. B. Atkinson<sup>1</sup>, J. G. Radney<sup>1,\*</sup>, J. Lum<sup>1</sup>, K. R. Kolesar<sup>2</sup>, D. J. Cziczo<sup>3</sup>,  
M. S. Pekour<sup>4</sup>, Q. Zhang<sup>5</sup>, A. Setyan<sup>5,\*\*</sup>, A. Zelenyuk<sup>4</sup>, and C. D. Cappa<sup>2</sup>

<sup>1</sup>Department of Chemistry, Portland State University, Portland, OR, 97207, USA

<sup>2</sup>Department of Civil and Environmental Engineering, University of California, Davis, CA, 95616, USA

<sup>3</sup>Earth, Atmosphere and Planetary Sciences, Massachusetts Institute of Technology, Cambridge, MA, 02139, USA

<sup>4</sup>Pacific Northwest National Laboratory, Richland, WA, 99352, USA

<sup>5</sup>Department of Environmental Toxicology, University of California, Davis, CA, 95616, USA

\* now at: Material Measurement Laboratory, National Institute of Standards and Technology, Gaithersburg, Maryland, 20899, USA

\*\* now at: Empa, Swiss Federal Laboratories for Materials Science and Technology, 8600 Dübendorf, Switzerland

Title Page

Abstract

Introduction

Conclusions

References

Tables

Figures



Back

Close

Full Screen / Esc

Printer-friendly Version

Interactive Discussion



Received: 11 October 2014 – Accepted: 11 November 2014 – Published: 10 December 2014

Correspondence to: D. B. Atkinson (atkinsdb@pdx.edu) or C. D. Cappa (cdcappa@ucdavis.edu)

Published by Copernicus Publications on behalf of the European Geosciences Union.

**ACPD**

14, 31203–31247, 2014

**Aerosol  
hygroscopicity  
measurements  
during CARES 2010**

D. B. Atkinson et al.

Title Page

Abstract

Introduction

Conclusions

References

Tables

Figures



Back

Close

Full Screen / Esc

Printer-friendly Version

Interactive Discussion



## Abstract

Measurements of the effect of water uptake on particulate light extinction or scattering made at two locations during the 2010 CARES study around Sacramento, CA are reported. The observed influence of water uptake, characterized through the dimensionless optical hygroscopicity parameter  $\gamma$ , is compared with calculations constrained by observed particle size distributions and size-dependent particle composition. A closure assessment has been carried out that allowed for determination of the average hygroscopic growth factors (GF) at 85 % relative humidity and the dimensionless hygroscopicity parameter  $\kappa$  for oxygenated organic aerosol (OA) and for supermicron particles, yielding  $\kappa = 0.1\text{--}0.15$  and  $0.9\text{--}1.0$ , respectively. The derived range of oxygenated OA  $\kappa$  values are in line with previous observations. The relatively large values for supermicron particles is consistent with substantial contributions of sea salt-containing particles in this size range. Analysis of time-dependent variations in the supermicron particle hygroscopicity suggest that atmospheric processing, specifically chloride displacement by nitrate and the accumulation of secondary organics on supermicron particles, can lead to substantial depression of the observed GF.

## 1 Introduction

It is well established that atmospheric particles can have a strong influence on climate through their direct effect: scattering and absorption of solar and terrestrial radiation. Models must incorporate the net counteracting effects of cooling due to light scattering by particles and warming due to light absorption by greenhouse gases and particles to be successful at predicting global mean temperature. Uncertainties associated with climate forcing by particles remain sizable, and the negative forcing may be comparable to the collective positive radiative forcing from greenhouse gases (IPCC, 2013). Refinements of the linkage between the end results of models and measurements – particulate optical effects on the climate system as observed by in situ, ground-based,

## Aerosol hygroscopicity measurements during CARES 2010

D. B. Atkinson et al.

Title Page

Abstract

Introduction

Conclusions

References

Tables

Figures



Back

Close

Full Screen / Esc

Printer-friendly Version

Interactive Discussion



remote, and satellite measurements – and the presumptive sources of the particles are desirable to allow prediction of the effects of regulatory and other changes in future emissions.

Global climate models cannot currently fully represent the complex mixing state of particles indicated by in situ measurements. Therefore, such models typically utilize compositionally ensemble-averaged particle types with defined size distributions to represent the contributions from various sources. At the other extreme, some detailed models used for regional climate modeling and air quality simulation account more explicitly for particle dynamics, aging and mixing state (e.g. Zaveri et al., 2010; Riemer et al., 2010). In both simple and complex models, the extent of particulate water is determined by the local atmospheric relative humidity (RH) and the particle composition, the latter of which controls the particle hygroscopicity.

Particle composition is variable in space and time. Ambient measurements of submicron particle (i.e., particles with diameters  $< 1 \mu\text{m}$ ) chemical composition indicate that both organic and inorganic components contribute substantially to the overall submicron particle burden (Jimenez et al., 2009). Compared to the major inorganic components, the properties of organic particulate matter – including hygroscopicity – are not as well established and are additionally much more variable. Much atmospheric organic particulate matter, or organic aerosol (OA), is secondary in origin, meaning that it is produced through chemical reactions. There are fewer studies that have explicitly investigated the hygroscopicity of ambient supermicron particles, i.e. those with diameters  $> 1 \mu\text{m}$  (e.g. Hegg et al., 2008; Zhang et al., 2014).

Particle hygroscopicity is commonly characterized through comparison between the light extinction or scattering coefficients ( $b_{\text{ext}}$  and  $b_{\text{scat}}$ , in  $\text{Mm}^{-1}$ ) measured at low (dry) and high relative humidity (RH). The extinction or scattering enhancement factors,  $f_{\text{ext}}(\text{RH})$  and  $f_{\text{scat}}(\text{RH})$ , are defined as the ratio between the  $b_{\text{ext}}$  or  $b_{\text{scat}}$  measured at the high and low RH values. There are many measurements of  $f(\text{RH})$  reported in the literature, often focusing on differences in observed  $f(\text{RH})$  values between air masses containing different aerosol types (e.g. marine, urban) (e.g. Zieger et al., 2010, 2013;

## Aerosol hygroscopicity measurements during CARES 2010

D. B. Atkinson et al.

Title Page

Abstract

Introduction

Conclusions

References

Tables

Figures



Back

Close

Full Screen / Esc

Printer-friendly Version

Interactive Discussion



---

**Aerosol  
hygroscopicity  
measurements  
during CARES 2010**D. B. Atkinson et al.

---

[Title Page](#)[Abstract](#)[Introduction](#)[Conclusions](#)[References](#)[Tables](#)[Figures](#)[Back](#)[Close](#)[Full Screen / Esc](#)[Printer-friendly Version](#)[Interactive Discussion](#)

Carrico et al., 2003; Massoli et al., 2009; Titos et al., 2014; Zhang et al., 2014). Yet new, quantitative assessments of the relationship(s) between particle composition and  $f$ (RH), and how these differ between different regions, remain necessary given that use of some of the most widely used aerosol optical models (e.g. OPAC) can still lead to substantial model/measurement discrepancies (Zieger et al., 2013). In particular, there remains a need to better understand the hygroscopic properties of OA and supermicron particles. In this study, the connections between particle composition, hygroscopicity, and optical properties (specifically scattering and extinction) are examined through optical closure based on observations made during the 2010 Carbonaceous Aerosols and Radiative Effects Study (CARES) field intensive (Zaveri et al., 2012). In particular, the observations are utilized to determine the hygroscopicity of specific particulate constituents, namely the oxygenated fraction of OA, termed OOA, and of supermicron particles.

## 2 CARES campaign

During June of 2010, a variety of aerosol and gas-phase species, as well as meteorological and radiative properties were measured as part of the CARES field intensive campaign in the Sacramento/Central Valley region of California (Zaveri et al., 2012). The CARES study was designed to take advantage of a persistent southwesterly flow pattern that transports pollutants from the Sacramento urban core and nearby Bay Area across the mostly agricultural areas in the Central Valley toward the forested foothills of the Sierra Nevada mountains (Fast et al., 2012). Two heavily instrumented ground sites were used to capture the evolution of the urban plume: one located just to the northeast of Sacramento, denoted T0, and one in the foothills of the Sierra Nevada in Cool, CA, referred to as T1 (Zaveri et al., 2012). Aircraft were also used to directly monitor the transport during periods predicted to have favorable meteorology. The results presented in this work are based on measurements obtained only at the two ground sites.

Much of the campaign was characterized by daytime west–east transport between the T0 and T1 sites, although there were occasional disruptions to the generalized flow pattern by shifts to northerly/northwesterly flow (Zaveri et al., 2012; Fast et al., 2012). The analysis here focuses primarily on periods with T0 → T1 transport, but data from the entire campaign are considered. At least one of these periods (near the end of June) exhibits multi-day recirculation, either as a result of a daytime upslope/nocturnal downslope flow pattern or involving airmass lofting followed by subsidence near the west side of the valley. The recirculation period produced an extensively processed organic aerosol (Setyan et al., 2012).

## 3 Experimental

### 3.1 Sampling

Instruments were housed in dual, air-conditioned construction trailers with common aerosol and gas-phase manifolds. The detailed specifications of the aerosol inlet system are provided in (Zaveri et al., 2012). Briefly, a high-throughput pump pulled air into a stainless steel aerosol inlet positioned between and above the trailers. The aerosol flow was split between the trailers and within the trailers into two separate 3/4 inch stainless manifolds connected to high-flow return pumps. Each aerosol instrument station accessed the manifold through a 1/4 inch centerline pick-off using the instrument's pumping system. No intentional size selection was incorporated into the aerosol sampling mast or manifold system, but some of the instruments used size fractionation at their individual sampling points, as noted below.

## Aerosol hygroscopicity measurements during CARES 2010

D. B. Atkinson et al.

Title Page

Abstract

Introduction

Conclusions

References

Tables

Figures



Back

Close

Full Screen / Esc

Printer-friendly Version

Interactive Discussion





## Aerosol hygroscopicity measurements during CARES 2010

D. B. Atkinson et al.

Title Page

Abstract

Introduction

Conclusions

References

Tables

Figures

◀

▶

◀

▶

Back

Close

Full Screen / Esc

Printer-friendly Version

Interactive Discussion



instruments were operated with one of two distinct configurations. In one (8–17 June), the three nephelometers were operated in parallel, with the aerosol stream being split and sampled respectively (i) through a Nafion dryer (low RH), (ii) without alteration (mid RH), and (iii) through a water-cooled line (high RH). In the second configuration (21–27 June), the entire aerosol stream was first humidified, after which 1/3 of the flow was split to a high-RH nephelometer and the remaining flow was passed through a Nafion dryer after which 1/2 of this flow was directed to a mid-RH nephelometer while the remaining flow was passed through a second Nafion drier and on to a low-RH nephelometer. The second configuration provided for more useful ranges of RH (since the original configuration often resulted in near-coincidence of the low and ambient RH channels) and assured that salt-like aerosols would be on the high RH branch (effluence) of the hysteresis curve. Measurements made using the second configuration are used in the primary analysis below, although results from 15 June (using the initial configuration) will be considered as a specific case study. The RH, temperature and pressure were measured independently by sensors within each of the nephelometers.

### 3.2.3 Hygroscopicity characterization

The low and highest RH  $b_{\text{ext}}$  and  $b_{\text{scat}}$  observations at T0 and T1, respectively, have been used to determine a time-series of  $f(\text{RH})$ . The  $f(\text{RH})$  values have been converted to the dimensionless extinction or scattering hygroscopicity parameters (Massoli et al., 2009; Quinn et al., 2005),  $\gamma_{\text{ext}}$  and  $\gamma_{\text{scat}}$ , as:

$$\gamma = - \frac{\ln[f(\text{RH})]}{\ln \left[ \frac{100 - \text{RH}_{\text{low}}}{100 - \text{RH}_{\text{high}}} \right]} \quad (1)$$

The use of  $\gamma$  assumes a power-law dependence of extinction and scattering on RH, which arises mostly from the increase in particle size with water uptake.  $\gamma$  also implicitly assumes continuous water uptake. Whereas  $f(\text{RH})$  is dependent on the absolute

RH values,  $\gamma$  is reasonably independent of RH and thus provides a more robust characterization of the fundamental particle hygroscopicity.

### 3.3 Particle composition measurements

#### 3.3.1 Ensemble aerosol mass spectrometry

5 Mass concentrations of submicron non-refractory particulate matter (NR-PM) were measured at both T0 and T1 using Aerodyne high resolution time-of-flight aerosol mass spectrometers (HR-ToF-AMS, henceforth AMS) (Canagaratna et al., 2007; DeCarlo et al., 2006). NR-PM components measured by the AMS include the major inorganic species sulfate, nitrate and ammonium (along with some forms of chlorine), and  
10 OA. The AMS measures ensemble-average particle composition for particles with vacuum aerodynamic diameters ( $d_{p,va}$ ) between  $\sim 30$  and 1000 nm. At T1, size-dependent composition was also measured. Assuming spherical particles,  $d_{p,va}$  is related to the particle mobility diameter ( $d_{p,m}$ ) through particle density  $\rho_p$  (assuming spherical particles) (DeCarlo et al., 2004). A  $d_{p,va} = 1000$  nm corresponds to a  $d_{p,m}$  of 670 nm for  
15  $\rho_p = 1.5 \text{ g cm}^{-3}$  and 500 nm for  $\rho_p = 2 \text{ g cm}^{-3}$ . The calculation of optical properties depends on geometric (physical) diameter, which for spherical particles is equal to  $d_{p,m}$  and not  $d_{p,va}$ . Therefore, with respect to the measurement of particle composition relevant to the calculation of optical properties, it is more precise to state that the AMS measures approximately sub-670 nm particles, not submicron particles. However, for simplicity and consistency with the literature we will refer to particles with  $d_{p,va} < 1000$  nm  
20 as submicron.

Further characterization of the OA was obtained via positive matrix factorization (PMF), from which different OA “types” (or factors) were identified (Zhang et al., 2011). During CARES, three major factors were identified at T0 and T1. At T0 there were  
25 two less-oxygenated factors and one highly oxygenated factor, while at T1 there was only one less-oxygenated factor but two highly oxygenated factors (Setyan et al., 2012). Since the hygroscopicity of the two less oxygenated OA factors at T0 and the two highly

## Aerosol hygroscopicity measurements during CARES 2010

D. B. Atkinson et al.

Title Page

Abstract

Introduction

Conclusions

References

Tables

Figures

⏪

⏩

◀

▶

Back

Close

Full Screen / Esc

Printer-friendly Version

Interactive Discussion







### 3.4 Size distribution measurements

Submicron dry particle mobility diameter ( $d_{p,m}$ ) size distributions were measured at T0 and T1 using scanning mobility particle sizers (SMPS) comprised of a charge neutralizer, differential mobility analyzer (DMA) and a condensation particle counter (CPC). The SMPS at T0 was a commercial TSI system (3081 DMA column and model 3775 CPC). The SMPS used at T1 is described in (Setyan et al., 2014). The SMPS data were corrected for multiply-charged particles and diffusional losses within the instruments. At T0 the SMPS was configured to measure particles over a size range of 12 to 737 nm while the T1 instrument measured from 8 to 858 nm.

Supermicron dry particle aerodynamic diameter ( $d_{p,a}$ ) size distributions were measured at both sites over the size range 542 to 20 000 nm using aerodynamic particle sizers (APS; Model 3321, TSI, Inc.). The measured aerodynamic size distributions were converted to  $d_{p,m}$  equivalent size distributions assuming spherical particles and a constant density of  $2.0 \text{ g cm}^{-3}$  (roughly compatible with either an inferred dust or sea salt composition) with:

$$d_{p,m} = d_{p,a} \sqrt{\frac{1}{\rho_p} \frac{C_c(d_{p,a})}{C_c(d_{p,m})}} \quad (2)$$

where  $C_c$  is the Cunningham slip correction factor (DeCarlo et al., 2004). Because  $C_c$  depends on  $d_{p,m}$ , Eq. (2) must be solved iteratively. For reference, a particle with  $d_{p,a} = 2500 \text{ nm}$  and  $\rho_p = 2 \text{ g cm}^{-3}$  has a  $d_{p,m} = 1745 \text{ nm}$  and a particle with  $d_{p,a} = 1000 \text{ nm}$  and  $2 \text{ g cm}^{-3}$  has a  $d_{p,m} = 685 \text{ nm}$ . It should be noted that  $d_{p,a}$  is not equivalent to the  $d_{p,va}$  measured by the AMS, SPLAT II and PALMS.

The SMPS and converted APS size distributions were merged into a single mobility-diameter size distribution (Fig. 1c and f). The SMPS measurements were used for particles with diameters  $< 737 \text{ nm}$  and the APS measurements were used for larger particles. We will refer to particles with  $d_{p,m} < 737 \text{ nm}$  as “submicron” and with  $1700 \text{ nm}$

## Aerosol hygroscopicity measurements during CARES 2010

D. B. Atkinson et al.

Title Page

Abstract

Introduction

Conclusions

References

Tables

Figures

◀

▶

◀

▶

Back

Close

Full Screen / Esc

Printer-friendly Version

Interactive Discussion



$d_{p,m} > 737$  nm as “supermicron”, since the sub/supermicron distinction is typically based on aerodynamic diameter.

The APS at T0 malfunctioned after 22 June 21:00 PST, limiting the period over which observations of extensive properties, such as  $b_{\text{ext}}$ , at this site can be directly compared with calculations. However, calculations of intensive properties, such as  $f(\text{RH})$  or  $\gamma_{\text{RH}}$ , exhibit less sensitivity to the exact nature of the size distribution since the intensive properties depend on the calculation of ratios of extensive properties; this is especially true when  $d_{p,m} \gtrsim 700$  nm. This lack of sensitivity is exploited here to facilitate comparison of calculated and observed  $\gamma_{\text{RH}}$ . The measured supermicron size distribution shape was constant in time over the measurement period during which the APS was operating properly, with only the total particle concentration varying. A synthetic supermicron size distribution for the missing data period was therefore determined by comparing the observed and calculated dry particle  $b_{\text{ext}}$  (see next section). Specifically, the shape of the distribution was assumed equal to the campaign average (Fig. S1), and the number concentration of particles with  $d_{p,m} > 737$  nm was scaled such that the observed and calculated dry  $b_{\text{ext}}$  agreed to within 1%. The final, merged size distribution after 22 June is comprised of actual SMPS measurements and the synthetic APS distribution. Importantly, small mismatches in the exact shape of the supermicron particle size distribution have only a small effect on the derived hygroscopicity.

## 4 Optical property calculations

### 4.1 General methodology

Time-series of  $b_{\text{ext}}$  and  $b_{\text{scat}}$  have been calculated from Mie theory for both low and high RH conditions using the measured dry particle size distribution and composition as model inputs. The combined low RH and high RH calculations have been used to calculate  $f(\text{RH})$  and  $\gamma$  values, which can be compared with the observations. The calculations require specification of the amount of particle phase water and the associated

## Aerosol hygroscopicity measurements during CARES 2010

D. B. Atkinson et al.

Title Page

Abstract

Introduction

Conclusions

References

Tables

Figures



Back

Close

Full Screen / Esc

Printer-friendly Version

Interactive Discussion





## Aerosol hygroscopicity measurements during CARES 2010

D. B. Atkinson et al.

Title Page

Abstract

Introduction

Conclusions

References

Tables

Figures

◀

▶

◀

▶

Back

Close

Full Screen / Esc

Printer-friendly Version

Interactive Discussion



components using the densities given in Table 1. Dry supermicron particles were assumed to have a constant real refractive index (Table 1). This assumption does not account for variations in the refractive index that can result from variations in the supermicron particle composition (e.g. sea salt vs. dust). Particulate water volume fractions ( $VF_{H_2O}$ ) were determined based on the measured particle composition, as discussed further below. The base-case assumes that the particles do not absorb light. The influence of particle light absorption on the calculations is discussed separately in Sect. 5.2.7.

The RH-specific physical growth factors ( $GF = d_{p,m,wet}/d_{p,m,dry}$ ) associated with each submicron NR-PM component ( $GF_i$ ) were determined based on the hygroscopicity parameter,  $\kappa$ , of the individual component using the relationship (Petters and Kreidenweis, 2007):

$$\frac{RH}{\exp\left(\frac{A}{d_{p,m,dry} \cdot GF}\right)} = \frac{GF^3 - 1}{GF^3 - (1 - \kappa)} \quad (5)$$

where  $d_{p,m,dry}$  is the dry particle diameter, RH is the measured (low or high) RH and  $A = 2.09$  nm is a constant that includes the surface tension of water and other physical constants. Values of  $\kappa$  for the inorganic salts, black carbon and HOA are specified based on the literature (Table 1), while  $\kappa$  values for both OOA and supermicron particles are determined through optical closure, discussed in Sect. 5.2. The overall GF of the particles at the measured RH were then calculated from volume mixing rules:

$$GF_{tot}(RH) = \left( \sum_i VF_i \cdot GF_i(RH) \right)^{\frac{1}{3}} \quad (6)$$

where the summation is taken over all non-water components. The wet particle diameters for use in the Mie calculations (Eq. 4) are

$$d_{p,m,RH} = GF_{tot}(RH) \cdot d_{p,m,dry}, \quad (7)$$





**Aerosol  
hygroscopicity  
measurements  
during CARES 2010**

D. B. Atkinson et al.

Title Page

Abstract

Introduction

Conclusions

References

Tables

Figures

◀

▶

◀

▶

Back

Close

Full Screen / Esc

Printer-friendly Version

Interactive Discussion



correspondence with OOA and HOA, respectively (Setyan et al., 2012). The bulk particle composition at each point in time was also determined from the AMS measurements, with the exception of BC, which comes from the SP2 measurements. The measured  $\text{NH}_4^+$  was apportioned on a molar basis between  $\text{NO}_3^-$ ,  $\text{SO}_4^{2-}$  and  $\text{Cl}^-$  to produce  $\text{NH}_4\text{NO}_3$ ,  $(\text{NH}_4)_2\text{SO}_4$  and  $\text{NH}_4\text{Cl}$ ; residual  $\text{NH}_4^+$  was negligible (Setyan et al., 2012).

As noted above, for T0 size-dependent submicron composition data from the AMS were not available. Therefore, the SPLAT II data were used to obtain the variation in composition with size within the submicron range and to determine the normalized size-dependent composition. To provide some consistency between T0 and T1, the SPLAT particle types were mapped onto the AMS+SP2-derived component types as follows: HOA is equivalent to the sum of the SPLAT II POA, BB, and HC categories; BC is equivalent to the SPLAT II soot type; inorganic ions (excluding sea salt and dust) are equivalent to SPLAT II sulfate; oxygenated OA is equivalent to SPLAT II OA. SPLAT II reports sulfate and OA as mixed particle types of varying relative composition, and thus the sulfate and OA modes were estimated from weighted sums of the mixed sulfate + OA particle types. For example, the size distribution for the 50/50 sulfate + OA mixed particle type is split into two individual sulfate and organic size distributions, with half the mass in one and half in the other. The total sulfate (really, total inorganics) and OA distributions are then determined from the sum over all of the different sulfate + OA particle types. The overall distribution is then determined by assuming that the particles are internally mixed within each size bin. A cartoon illustrating this process is shown in Fig. S2. This last assumption (internal mixing within a given size bin) discards some of the available information from the SPLAT II measurements on mixing state, but is done to facilitate comparison with the AMS results from T1. Comparison of the size-independent internally-mixed vs. externally-mixed calculations provides some indication of the limitations of this simplification.

It is assumed in all cases that the supermicron composition is size-independent, a simplification that has been made to account for limitations regarding time-dependent variations in the supermicron particle composition. Unless otherwise stated, results of

calculations in Sect. 5.2 have used the size-dependent submicron composition method. The three approaches (external mixing, size-independent internally mixed and size-dependent internally mixed) are compared in Sect. 5.2.6.

## 5 Results and discussion

### 5.1 Overview of observations

Time series for the dried ( $RH < 40\%$ ) and humidified ( $RH \sim 85\%$ ) particle extinction (532 nm) or scattering (525 nm), the submicron particle composition as volume fractions, and the volume-weighted particle size distributions are shown in Fig. 1 for both T0 and T1. At T1 the submicron particle composition is dominated by OOA (Fig. 1e), as noted by Setyan et al. (2012). At T0, organics also comprise a large fraction of the total submicron PM, although HOA/OA is larger than at T1 (Fig. 1b). Further, there are periods where the OA fraction is only  $\sim 50\%$  of the submicron PM mass at T0, while the OA fraction is always  $> 70\%$  at T1. At both T0 and T1 the submicron contribution to the overall  $PM_{2.5}$  particle volume concentration tends to be larger than for supermicron components, although there are periods where the supermicron components contribute substantially (Figs. 1c and f and S3), and it should be noted that contributions from even larger particles ( $d_{p,a} > 2.5 \mu m$ ) can be substantial (Kassianov et al., 2012).

Time-series of the observed optical hygroscopicity parameter,  $\gamma$ , for T0 and T1 are shown in Fig. 3a and c. Values of  $\gamma$  varied from as low as  $\sim 0.2$  to as high as  $\sim 1.0$ . The values of  $\gamma$  at T0 and T1 are similar during the latter part of the study (22 through 28 June) when transport and recirculation is thought to have homogenized the particle composition between the two sites (Zaveri et al., 2012; Fast et al., 2012).

## Aerosol hygroscopicity measurements during CARES 2010

D. B. Atkinson et al.

Title Page

Abstract

Introduction

Conclusions

References

Tables

Figures



Back

Close

Full Screen / Esc

Printer-friendly Version

Interactive Discussion



## 5.2 Optical property model/measurement comparison

### 5.2.1 Optical closure under low-humidity conditions

Time-series of  $b_{\text{ext, low}}$  and  $b_{\text{sca, low}}$  for  $\text{PM}_{2.5}$  and  $\text{PM}_1$  have been calculated from Mie theory, with the  $\text{PM}_{2.5}$  results shown in Fig. 3. There is generally good agreement between the measured and calculated  $b_{\text{ext, low}}$  or  $b_{\text{sca, low}}$  (Fig. 4a and b) at both sites. The slope of a linear Orthogonal Distance Regression (ODR) fit of the observed vs. calculated  $b_{\text{ext, low}}$  at T0 is  $1.005 (\pm 0.005)$  ( $1\sigma$  of the fit) and for the  $b_{\text{sca, low}}$  at T1 is  $1.02 (\pm 0.004)$ , which demonstrates agreement and closure to well within the experimental uncertainties. (Note that for T0, only data from the period prior to 6/22 at 21:00 PST, when the APS was in operation, are included in the fit.) The generally good agreement at T1 is notable since no explicit size cut was used during sampling and is important in the context of the particle hygroscopicity assessment discussed below. For these fits (Fig. 4a and b), the y-intercept was constrained to be equal to zero, but the intercepts produced when the fits were not forced through zero were statistically indistinguishable from zero at the 95 % confidence level.

The calculated average supermicron fractional contribution ( $f_{\text{super}}$ ) to the  $\text{PM}_{2.5}$   $b_{\text{ext}}$  at T0 ranged from 0.05 to 0.4, with a mean value of  $0.21 \pm 0.10$  ( $1\sigma$ ), while at T1  $f_{\text{super}}$  ranged from 0.05 to 0.6 with a mean value of  $0.22 \pm 0.13$  ( $1\sigma$ ) (Fig. S3). The  $f_{\text{super}}$  at T1 after 21 June (i.e. during the period when reliable high RH measurements are available) were smaller, varying from 0.05 to 0.4 with a mean of  $0.11 \pm 0.05$  ( $1\sigma$ ) (Fig. S3). There is a general correspondence between periods of high supermicron influence at T0 and T1, in particular during the period from 18 to 21 June, although the  $f_{\text{super}}$  values at T1 tend to lag those at T0 by 6–12 h.

### 5.2.2 Optical closure under elevated-humidity conditions

The calculation of wet particle optical properties requires that the GF (or equivalently  $\kappa$  values) for the major PM components are known so that the water uptake due to

## Aerosol hygroscopicity measurements during CARES 2010

D. B. Atkinson et al.

Title Page

Abstract

Introduction

Conclusions

References

Tables

Figures



Back

Close

Full Screen / Esc

Printer-friendly Version

Interactive Discussion





coefficients are compared to the measurements in Fig. 4c and d. (Time-series of the RH in the high RH channels, and the associated  $f(\text{RH})$  are shown in Fig. S4.) The overall model/measurement agreement in the calculated extensive optical properties is good, with slopes of 0.992 ( $\pm 0.004$ ) ( $1\sigma$  of the fit) at T0 and 1.03 ( $\pm 0.004$ ) at T1.

5 This good agreement is as expected given the model/measurement agreement under low RH conditions and the fact that the  $\kappa_{\text{OOA}}$  and  $\kappa_{\text{super}}$  were optimized to give good model/measurement in  $\gamma$ .

### 5.2.3 Oxygenated organic aerosol hygroscopicity

The optimal average OOA hygroscopicities are  $\kappa_{\text{OOA}} = 0.15 \pm 0.04$  for T0 and  $0.09 \pm 0.03$  for T1. The uncertainty estimate is discussed in Sect. 5.2.5. There is some cross-sensitivity to the optimization results, e.g. larger values of  $\kappa_{\text{super}}$  lead to smaller values of  $\kappa_{\text{OOA}}$ , and vice versa. However, the particular cross-sensitivities of  $\kappa_{\text{super}}$  and  $\kappa_{\text{OOA}}$  differ between the two sites. At T0 the optimal  $\kappa_{\text{super}}$  exhibits relatively small sensitivity to the  $\kappa_{\text{OOA}}$ , while the reverse is not true. At T1 the optimal  $\kappa_{\text{super}}$  exhibits greater sensitivity to variations in the  $\kappa_{\text{OOA}}$ , with the  $\kappa_{\text{OOA}}$  reasonably independent of  $\kappa_{\text{super}}$ . These differences in cross-sensitivity between the two sites arise from differences in particle composition and the relative contributions of sub- and supermicron particles to the total extinction or scattering. At T0 the supermicron contribution to total extinction is substantial while at T1 it is relatively small over the period considered. At T1 the overall scattering is dominated by OOA, while at T0 the OOA contribution, although not insignificant, is comparably smaller.

The consistency of the derived  $\kappa_{\text{OOA}}$  between the two sites suggests that for OOA in the Sacramento region in the summer is  $\kappa_{\text{OOA}} \sim 0.09\text{--}0.15$ , although the optimal  $\kappa_{\text{OOA}}$  derived for T1 is likely more robust than that at T0 because of the greater sensitivity of  $\kappa_{\text{OOA}}$  to  $\kappa_{\text{super}}$  at T0. The oxygen-to-carbon atomic ratio (O : C) for OOA at T1 was  $\sim 0.5$  (Setyan et al., 2012) and, although comparable values are unavailable for the T0 site, the aircraft measurements indicated O : C for OOA is  $\sim 0.6$  over the Sacramento region in general (Shilling et al., 2013). Previous work suggests that there is some relation-

## Aerosol hygroscopicity measurements during CARES 2010

D. B. Atkinson et al.

Title Page

Abstract

Introduction

Conclusions

References

Tables

Figures



Back

Close

Full Screen / Esc

Printer-friendly Version

Interactive Discussion





## Aerosol hygroscopicity measurements during CARES 2010

D. B. Atkinson et al.

Title Page

Abstract

Introduction

Conclusions

References

Tables

Figures



Back

Close

Full Screen / Esc

Printer-friendly Version

Interactive Discussion



spectrometry results indicate that there are some variations in the supermicron particle composition, which could lead to temporal variations in  $\kappa_{\text{super}}$ . The potential variability in  $\kappa_{\text{super}}$  has been assessed by minimizing the difference between the modeled and measured  $\gamma_{\text{ext}}$  and  $\gamma_{\text{sca}}$  at every point in time while holding  $\kappa_{\text{OOA}}$  constant at 0.15, as opposed to a single campaign average value. A histogram of the derived individual  $\kappa_{\text{super}}$  values for the T0 site shows a broad distribution centered around 0.8 (Fig. S5). (The T0 site was considered here since the supermicron contribution to scattering at this site was larger. Also, use of a different  $\kappa_{\text{OOA}}$  would shift the distribution, but have minimal influence on the spread.) Assessing variability in  $\kappa_{\text{super}}$  by setting  $\kappa_{\text{OOA}}$  to be constant is reasonable given the similarity between the  $\kappa_{\text{OOA}}$  values at T0 and T1 and with literature values.

Variability in the supermicron composition could result from variations in sources of primary supermicron PM or from photochemical processing. Sacramento is located about 90 miles from the San Francisco Bay and Pacific Ocean, and thus sea-spray particles transported to the T0 site in Sacramento and the T1 site in the Sierra Foothills will likely have undergone some photochemical processing along the way. As noted above, sea salt-containing particles make up a substantial proportion of supermicron particles sampled during the measurement period (Fig. 6). The majority of the sea salt particles observed were processed to differing extents as indicated in the single particle mass spectra by the presence of characteristic peaks for NaCl ( $m/z$  23, 81, 83) and NaNO<sub>3</sub> ( $m/z$  23, 62, 30, 39, 78, 92, 108) with different relative intensities. Displacement of chloride with nitrate as a result of HNO<sub>3</sub> uptake on sea salt containing particles (Gard et al., 1998) would lead to a decrease in the overall particle hygroscopicity since  $\kappa_{\text{NaNO}_3} \sim 0.84 < \kappa_{\text{NaCl}} \sim 1.2$  (Petters and Kreidenweis, 2007). Similarly, the addition of secondary organic material would lead to a decrease in  $\kappa$  relative to that for fresh sea salt, since  $\kappa_{\text{OOA}} < \kappa_{\text{NaNO}_3} < \kappa_{\text{NaCl}}$ . Thus, although classified simply as “sea salt”, more detailed consideration of the mass spectra associated with these sodium-containing particles indicate compositional variations associated with photochemical processing, with both nitrate and organic signatures observed.





overall uncertainty for  $\kappa_{\text{OOA}}$  at T1 is determined predominately by the RH uncertainty. The supermicron contribution to  $b_{\text{ext}}$  at T1 is comparably small, making  $\kappa_{\text{super}}$  much more sensitive to variations in the other  $\kappa$  values compared to T0. Specifically,  $\kappa_{\text{super}}$  is highly dependent on the  $\kappa_{\text{AS}}$ , changing by 0.12 for a 10 % change in  $\kappa_{\text{AS}}$ . The estimated uncertainty in  $\kappa_{\text{super}}$  from the cross-sensitivity to  $\kappa_{\text{OOA}}$  is 0.1. Thus, for T1, the mean values for the OOA and supermicron hygroscopicity are  $\kappa_{\text{OOA}} = 0.09 \pm 0.03$  and  $\kappa_{\text{super}} = 1.0 \pm 0.2$ .

### 5.2.6 Influence of assumed mixing state

Three different models of the submicron particle mixing state were tested in calculating the particle optical properties: an internal mixture with size-dependent composition (the base case discussed above), an internal mixture with size-independent composition and an external mixture with size-dependent composition. The optimization procedure was repeated for the two alternative models. The derived optimal  $\kappa_{\text{OOA}}$  values are 0.15, 0.13, and 0.10 for T0 and 0.09, 0.16 and 0.08 for T1 for the internal + size-dependent composition, internal + size-independent composition and external mixture models, respectively. It is apparent that the derived  $\kappa_{\text{OOA}}$  exhibits some, albeit limited sensitivity to the assumed mixing state, at least for the particle distributions in the Sacramento region in the summer. The derived optimal  $\kappa_{\text{super}}$  values are 0.9, 1.2 and 0.8 for T0 and 1.0, 1.1 and 0.9 for T1 for the internal + size-dependent, internal + size-independent and external mixture models, respectively. Like  $\kappa_{\text{OOA}}$ , the derived  $\kappa_{\text{super}}$  is not strongly dependent upon the model formulation, although because the supermicron particles are treated as a separate, internally mixed mode in all cases this is perhaps to be expected. Despite the similarity of the derived  $\kappa_{\text{OOA}}$  and  $\kappa_{\text{super}}$  values between the three models, the two size-dependent composition models generally resulted in more definitive retrievals of the hygroscopicities, i.e. the calculated  $\chi^2$  values exhibited a more well-defined minimum. This suggests that accounting for differences in the size distributions of inorganic and organic components may be important for accurate calculation of the optical properties of ambient PM at elevated RH.

## Aerosol hygroscopicity measurements during CARES 2010

D. B. Atkinson et al.

Title Page

Abstract

Introduction

Conclusions

References

Tables

Figures



Back

Close

Full Screen / Esc

Printer-friendly Version

Interactive Discussion





**Aerosol  
hygroscopicity  
measurements  
during CARES 2010**

D. B. Atkinson et al.

Title Page

Abstract

Introduction

Conclusions

References

Tables

Figures



Back

Close

Full Screen / Esc

Printer-friendly Version

Interactive Discussion

tively. These test calculations indicate that the neglect of absorption by BC will have had a minimal influence on the  $\gamma_{\text{ext}}$  calculations, and consequently on the derived  $\kappa_{\text{OOA}}$  and  $\kappa_{\text{super}}$  at the T0 site. In contrast, the calculated  $\gamma_{\text{sca}}$  without absorption might be biased low by a small amount, which could consequently lead to small low biases in the calculated  $\kappa_{\text{OOA}}$  and  $\kappa_{\text{super}}$  at the T1 site.

## 6 Conclusions

Measurements of light extinction and light scattering by ambient particles ( $\text{PM}_{2.5}$ ) were made at two sites under low and high RH conditions during the 2010 CARES campaign in Sacramento, CA to assess the influence of water uptake on the optical properties of the particles. The overall effect of water uptake on extinction and scattering was characterized by the optical hygroscopicity parameter  $\gamma$ . Concurrent measurements of particle composition allowed for assessment of the relationship between particle composition and the water uptake. Optical closure calculations for the low RH measurements indicate good model/measurement agreement when the model is constrained by observed size distributions. Effective hygroscopicities, i.e.  $\kappa$  values, were determined for OOA and for supermicron (defined here as particles with  $1 \mu\text{m} < d_{\text{p,a}} < 2.5 \mu\text{m}$ ) particles based on comparison between observed and calculated  $\gamma$  values. The derived campaign-average  $\kappa_{\text{OOA}}$  values at the two sites were similar, with  $\kappa_{\text{OOA}} = 0.15 \pm 0.04$  (T0) and  $0.09 \pm 0.03$  (T1), indicating that OOA is moderately hygroscopic, consistent with previous studies. The derived campaign-average  $\kappa_{\text{super}}$  values at the two sites were also similar to each other, with  $\kappa_{\text{super}} = 0.9 \pm 0.2$  (T0) and  $1.0 \pm 0.2$  (T1), indicating that the supermicron particles in this region were overall highly hygroscopic. However, the  $\kappa_{\text{super}}$  exhibited some dependence on the particle composition, with larger values observed when the supermicron particles were dominated by sea salt and smaller values observed as chloride was replaced by nitrate or when supermicron organics were prevalent.

*Acknowledgements.* DBA, CDC and QZ were supported by of the Office of Science (BER), US Department of Energy (DOE), Atmospheric System Research Program through Grants No. DE-SC0008937 and DE-FG02-11ER65293. The authors thank R. Subramanian for use of the SP2 data. Additional funding for data collection at the ground sites (including of the SP2 data) was provided by the Atmospheric Radiation Measurement (ARM) Program of the US DOE, Office of Biological and Environmental Research (OBER).

## References

- Bohren, C. F. and Huffman, D. R.: Absorption and Scattering of Light by Small Particles, Wiley, New York, xiv, 350 pp., 1983.
- Bond, T. C., Habib, G., and Bergstrom, R. W.: Limitations in the enhancement of visible light absorption due to mixing state, *J. Geophys. Res.-Atmos.*, 111, doi:10.1029/2006JD007315, 2006.
- Canagaratna, M. R., Jayne, J. T., Jimenez, J. L., Allan, J. D., Alfarra, M. R., Zhang, Q., Onasch, T. B., Drewnick, F., Coe, H., Middlebrook, A., Delia, A., Williams, L. R., Trimborn, A. M., Northway, M. J., DeCarlo, P. F., Kolb, C. E., Davidovits, P., and Worsnop, D. R.: Chemical and microphysical characterization of ambient aerosols with the aerodyne aerosol mass spectrometer, *Mass Spectrom. Rev.*, 26, 185–222, doi:10.1002/mas.20115, 2007.
- Cappa, C. D., Che, D. L., Kessler, S. H., Kroll, J. H., and Wilson, K. R.: Variations in organic aerosol optical and hygroscopic properties upon heterogeneous OH oxidation, *J. Geophys. Res.-Atmos.*, 116, D15204, doi:10.1029/2011jd015918, 2011.
- Cappa, C. D., Onasch, T. B., Massoli, P., Worsnop, D., Bates, T. S., Cross, E., Davidovits, P., Hakala, J., Hayden, K., Jobson, B. T., Kolesar, K. R., Lack, D. A., Lerner, B., Li, S. M., Mellon, D., Nuaanman, I., Olfert, J., Petaja, T., Quinn, P. K., Song, C., Subramanian, R., Williams, E. J., and Zaveri, R. A.: Radiative absorption enhancements due to the mixing state of atmospheric black carbon, *Science*, 337, 1078–1081, doi:10.1126/science.1223447, 2012.

**Aerosol  
hygroscopicity  
measurements  
during CARES 2010**

D. B. Atkinson et al.

Title Page

Abstract

Introduction

Conclusions

References

Tables

Figures



Back

Close

Full Screen / Esc

Printer-friendly Version

Interactive Discussion



Cappa, C. D., Williams, E. J., Lack, D. A., Buffaloe, G. M., Coffman, D., Hayden, K. L., Herndon, S. C., Lerner, B. M., Li, S.-M., Massoli, P., McLaren, R., Nuaaman, I., Onasch, T. B., and Quinn, P. K.: A case study into the measurement of ship emissions from plume intercepts of the NOAA ship *Miller Freeman*, *Atmos. Chem. Phys.*, 14, 1337–1352, doi:10.5194/acp-14-1337-2014, 2014.

Carrico, C. M., Kus, P., Rood, M. J., Quinn, P. K., and Bates, T. S.: Mixtures of pollution, dust, sea salt, and volcanic aerosol during ACE-Asia: radiative properties as a function of relative humidity, *J. Geophys. Res.-Atmos.*, 108, 8650, doi:10.1029/2003JD003405, 2003.

Chang, R. Y.-W., Slowik, J. G., Shantz, N. C., Vlasenko, A., Liggio, J., Sjostedt, S. J., Leaitch, W. R., and Abbatt, J. P. D.: The hygroscopicity parameter ( $\kappa$ ) of ambient organic aerosol at a field site subject to biogenic and anthropogenic influences: relationship to degree of aerosol oxidation, *Atmos. Chem. Phys.*, 10, 5047–5064, doi:10.5194/acp-10-5047-2010, 2010.

Cziczo, D. J., Thomson, D. S., Thompson, T. L., DeMott, P. J., and Murphy, D. M.: Particle analysis by laser mass spectrometry (PALMS) studies of ice nuclei and other low number density particles, *Int. J. Mass Spectrom.*, 258, 21–29, doi:10.1016/j.ijms.2006.05.013, 2006.

DeCarlo, P. F., Slowik, J. G., Worsnop, D., Davidovits, P., and Jimenez, J. L.: Particle morphology and density characterization by combined mobility and aerodynamic diameter measurements. Part 1: Theory, *Aerosol Sci. Tech.*, 38, 1185–1205, doi:10.1080/027868290903907, 2004.

DeCarlo, P. F., Kimmel, J. R., Trimborn, A., Northway, M. J., Jayne, J. T., Aiken, A. C., Gonin, M., Fuhrer, K., Horvath, T., Docherty, K. S., Worsnop, D. R., and Jimenez, J. L.: Field-deployable, high-resolution, time-of-flight aerosol mass spectrometer, *Anal. Chem.*, 78, 8281–8289, doi:10.1021/ac061249n, 2006.

Fast, J. D., Gustafson Jr., W. I., Berg, L. K., Shaw, W. J., Pekour, M., Shrivastava, M., Barnard, J. C., Ferrare, R. A., Hostetler, C. A., Hair, J. A., Erickson, M., Jobson, B. T., Flowers, B., Dubey, M. K., Springston, S., Pierce, R. B., Dolislager, L., Pederson, J., and Zaveri, R. A.: Transport and mixing patterns over Central California during the carbonaceous aerosol and radiative effects study (CARES), *Atmos. Chem. Phys.*, 12, 1759–1783, doi:10.5194/acp-12-1759-2012, 2012.

Fuller, K. A., Malm, W. C., and Kreidenweis, S. M.: Effects of mixing on extinction by carbonaceous particles, *J. Geophys. Res.-Atmos.*, 104, 15941–15954, doi:10.1029/1998jd100069, 1999.

**Aerosol  
hygroscopicity  
measurements  
during CARES 2010**

D. B. Atkinson et al.

Title Page

Abstract

Introduction

Conclusions

References

Tables

Figures



Back

Close

Full Screen / Esc

Printer-friendly Version

Interactive Discussion



Gard, E. E., Kleeman, M. J., Gross, D. S., Hughes, L. S., Allen, J. O., Morrical, B. D., Ferguson, D. P., Dienes, T., Gälli, E. M., Johnson, R. J., Cass, G. R., and Prather, K. A.: Direct observation of heterogeneous chemistry in the atmosphere, *Science*, 279, 1184–1187, doi:10.1126/science.279.5354.1184, 1998.

5 Hegg, D. A., Covert, D. S., and Jonsson, H. H.: Measurements of size-resolved hygroscopicity in the California coastal zone, *Atmos. Chem. Phys.*, 8, 7193–7203, doi:10.5194/acp-8-7193-2008, 2008.

IPCC: Climate Change: The Physical Science Basis. Contribution of Working Group I to the Fifth Assessment Report of the Intergovernmental Panel on Climate Change, edited by: Stocker, T. F., Qin, D., Plattner, G.-K., Tignor, M., Allen, S. K., Boschung, J., Nauels, A., Xia, Y., Bex, V., and Midgley, P. M., Cambridge University Press, Cambridge, UK, New York, NY, USA, 1535 pp., 2013.

10 Jimenez, J. L., Canagaratna, M. R., Donahue, N. M., Prevot, A. S. H., Zhang, Q., Kroll, J. H., DeCarlo, P. F., Allan, J. D., Coe, H., Ng, N. L., Aiken, A. C., Docherty, K. S., Ulbrich, I. M., Grieshop, A. P., Robinson, A. L., Duplissy, J., Smith, J. D., Wilson, K. R., Lanz, V. A., Hueglin, C., Sun, Y. L., Tian, J., Laaksonen, A., Raatikainen, T., Rautiainen, J., Vaattovaara, P., Ehn, M., Kulmala, M., Tomlinson, J. M., Collins, D. R., Cubison, M. J., Dunlea, E. J., Huffman, J. A., Onasch, T. B., Alfarra, M. R., Williams, P. I., Bower, K., Kondo, Y., Schneider, J., Drewnick, F., Borrmann, S., Weimer, S., Demerjian, K., Salcedo, D., Cottrell, L., Griffin, R., Takami, A., Miyoshi, T., Hatakeyama, S., Shimono, A., Sun, J. Y., Zhang, Y. M., Dzepina, K., Kimmel, J. R., Sueper, D., Jayne, J. T., Herndon, S. C., Trimborn, A. M., Williams, L. R., Wood, E. C., Middlebrook, A. M., Kolb, C. E., Baltensperger, U., and Worsnop, D. R.: Evolution of organic aerosols in the atmosphere, *Science*, 326, 1525–1529, doi:10.1126/science.1180353, 2009.

15 25 Kassianov, E., Pekour, M., and Barnard, J.: Aerosols in central California: unexpectedly large contribution of coarse mode to aerosol radiative forcing, *Geophys. Res. Lett.*, 39, L20806, doi:10.1029/2012GL053469, 2012.

Koehler, K. A., Kreidenweis, S. M., DeMott, P. J., Petters, M. D., Prenni, A. J., and Carrico, C. M.: Hygroscopicity and cloud droplet activation of mineral dust aerosol, *Geophys. Res. Lett.*, 36, L08805, doi:10.1029/2009GL037348, 2009.

30 Laborde, M., Mertes, P., Zieger, P., Dommen, J., Baltensperger, U., and Gysel, M.: Sensitivity of the Single Particle Soot Photometer to different black carbon types, *Atmos. Meas. Tech.*, 5, 1031–1043, doi:10.5194/amt-5-1031-2012, 2012a.

**Aerosol  
hygroscopicity  
measurements  
during CARES 2010**

D. B. Atkinson et al.

Title Page

Abstract

Introduction

Conclusions

References

Tables

Figures



Back

Close

Full Screen / Esc

Printer-friendly Version

Interactive Discussion

- Laborde, M., Schnaiter, M., Linke, C., Saathoff, H., Naumann, K.-H., Möhler, O., Berlenz, S., Wagner, U., Taylor, J. W., Liu, D., Flynn, M., Allan, J. D., Coe, H., Heimerl, K., Dahlkötter, F., Weinzierl, B., Wollny, A. G., Zanatta, M., Cozic, J., Laj, P., Hitzengerger, R., Schwarz, J. P., and Gysel, M.: Single Particle Soot Photometer intercomparison at the AIDA chamber, *Atmos. Meas. Tech.*, 5, 3077–3097, doi:10.5194/amt-5-3077-2012, 2012b.
- Lambe, A. T., Onasch, T. B., Massoli, P., Croasdale, D. R., Wright, J. P., Ahern, A. T., Williams, L. R., Worsnop, D. R., Brune, W. H., and Davidovits, P.: Laboratory studies of the chemical composition and cloud condensation nuclei (CCN) activity of secondary organic aerosol (SOA) and oxidized primary organic aerosol (OPOA), *Atmos. Chem. Phys.*, 11, 8913–8928, doi:10.5194/acp-11-8913-2011, 2011.
- Langridge, J. M., Richardson, M. S., Lack, D., Law, D., and Murphy, D. M.: Aircraft instrument for comprehensive characterization of aerosol optical properties, Part I: Wavelength-dependent optical extinction and its relative humidity dependence measured using Cavity Ringdown Spectroscopy, *Aerosol Sci. Tech.*, 45, 1305–1318, doi:10.1080/02786826.2011.592745, 2011.
- Levin, E. J. T., Prenni, A. J., Palm, B. B., Day, D. A., Campuzano-Jost, P., Winkler, P. M., Kreidenweis, S. M., DeMott, P. J., Jimenez, J. L., and Smith, J. N.: Size-resolved aerosol composition and its link to hygroscopicity at a forested site in Colorado, *Atmos. Chem. Phys.*, 14, 2657–2667, doi:10.5194/acp-14-2657-2014, 2014.
- Massoli, P., Bates, T. S., Quinn, P. K., Lack, D. A., Baynard, T., Lerner, B. M., Tucker, S. C., Brioude, J., Stohl, A., and Williams, E. J.: Aerosol optical and hygroscopic properties during TexAQS-GoMACCS 2006 and their impact on aerosol direct radiative forcing, *J. Geophys. Res.-Atmos.*, 114, D00f07, doi:10.1029/2008jd011604, 2009.
- Massoli, P., Lambe, A. T., Ahern, A. T., Williams, L. R., Ehn, M., Mikkila, J., Canagaratna, M. R., Brune, W. H., Onasch, T. B., Jayne, J. T., Petaja, T., Kulmala, M., Laaksonen, A., Kolb, C. E., Davidovits, P., and Worsnop, D. R.: Relationship between aerosol oxidation level and hygroscopic properties of laboratory generated secondary organic aerosol (SOA) particles, *Geophys. Res. Lett.*, 37, L24801, doi:10.1029/2010GL045258, 2010.
- Mei, F., Hayes, P. L., Ortega, A., Taylor, J. W., Allan, J. D., Gilman, J., Kuster, W., de Gouw, J., Jimenez, J. L., and Wang, J.: Droplet activation properties of organic aerosols observed at an urban site during CalNex-LA, *J. Geophys. Res.-Atmos.*, 118, 2903–2917, doi:10.1002/jgrd.50285, 2013.

## Aerosol hygroscopicity measurements during CARES 2010

D. B. Atkinson et al.

Title Page

Abstract

Introduction

Conclusions

References

Tables

Figures



Back

Close

Full Screen / Esc

Printer-friendly Version

Interactive Discussion



Mikhailov, E. F., Vlasenko, S. S., Podgorny, I. A., Ramanathan, V., and Corrigan, C. E.: Optical properties of soot–water drop agglomerates: an experimental study, *J. Geophys. Res.-Atmos.*, 111, D07209, doi:10.1029/2005JD006389, 2006.

Murphy, D. M., Cziczo, D. J., Froyd, K. D., Hudson, P. K., Matthew, B. M., Middlebrook, A. M., Peltier, R. E., Sullivan, A., Thomson, D. S., and Weber, R. J.: Single-particle mass spectrometry of tropospheric aerosol particles, *J. Geophys. Res.-Atmos.*, 111, doi:10.1029/2006JD007340, 2006.

Pekour, M. S., Schmid, B., Chand, D., Hubbe, J. M., Kluzek, C. D., Nelson, D. A., Tomlinson, J. M., and Cziczo, D. J.: Development of a New Airborne Humidigraph System, *Aerosol Sci. Tech.*, 47, 201–207, doi:10.1080/02786826.2012.741274, 2012.

Petters, M. D. and Kreidenweis, S. M.: A single parameter representation of hygroscopic growth and cloud condensation nucleus activity, *Atmos. Chem. Phys.*, 7, 1961–1971, doi:10.5194/acp-7-1961-2007, 2007.

Prather, K. A., Bertram, T. H., Grassian, V. H., Deane, G. B., Stokes, M. D., DeMott, P. J., Aluwihare, L. I., Palenik, B. P., Azam, F., Seinfeld, J. H., Moffet, R. C., Molina, M. J., Cappa, C. D., Geiger, F. M., Roberts, G. C., Russell, L. M., Ault, A. P., Baltrusaitis, J., Collins, D. B., Corrigan, C. E., Cuadra-Rodriguez, L. A., Ebben, C. J., Forestieri, S. D., Guasco, T. L., Hersey, S. P., Kim, M. J., Lambert, W. F., Modini, R. L., Mui, W., Pedler, B. E., Ruppel, M. J., Ryder, O. S., Schoepp, N. G., Sullivan, R. C., and Zhao, D. F.: Bringing the ocean into the laboratory to probe the chemical complexity of sea spray aerosol, *P. Natl. Acad. Sci. USA*, 110, 7550–7555, doi:10.1073/pnas.1300262110, 2013.

Quinn, P. K., Bates, T. S., Baynard, T., Clarke, A. D., Onasch, T. B., Wang, W., Rood, M. J., Andrews, E., Allan, J., Carrico, C. M., Coffman, D., and Worsnop, D.: Impact of particulate organic matter on the relative humidity dependence of light scattering: a simplified parameterization, *Geophys. Res. Lett.*, 32, doi:10.1029/2005GL024322, 2005.

Riener, N., West, M., Zaveri, R., and Easter, R.: Estimating black carbon aging time-scales with a particle-resolved aerosol model, *J. Aerosol Sci.*, 41, 143–158, doi:10.1016/j.jaerosci.2009.08.009, 2010.

Schnaiter, M., Linke, C., Mohler, O., Naumann, K. H., Saathoff, H., Wagner, R., Schurath, U., and Wehner, B.: Absorption amplification of black carbon internally mixed with secondary organic aerosol, *J. Geophys. Res.-Atmos.*, 110, doi:10.1029/2005JD006046, 2005.

Schwarz, J. P., Spackman, J. R., Gao, R. S., Perring, A. E., Cross, E., Onasch, T. B., Ahern, A., Wrobel, W., Davidovits, P., Olfert, J., Dubey, M. K., Mazzoleni, C., and Fahey, D. W.: The

## Aerosol hygroscopicity measurements during CARES 2010

D. B. Atkinson et al.

Title Page

Abstract

Introduction

Conclusions

References

Tables

Figures



Back

Close

Full Screen / Esc

Printer-friendly Version

Interactive Discussion



detection efficiency of the Single Particle Soot Photometer, *Aerosol Sci. Tech.*, 44, 612–628, doi:10.1080/02786826.2010.481298, 2010.

Setyan, A., Zhang, Q., Merkel, M., Knighton, W. B., Sun, Y., Song, C., Shilling, J. E., Onasch, T. B., Herndon, S. C., Worsnop, D. R., Fast, J. D., Zaveri, R. A., Berg, L. K., Wiedensohler, A., Flowers, B. A., Dubey, M. K., and Subramanian, R.: Characterization of submicron particles influenced by mixed biogenic and anthropogenic emissions using high-resolution aerosol mass spectrometry: results from CARES, *Atmos. Chem. Phys.*, 12, 8131–8156, doi:10.5194/acp-12-8131-2012, 2012.

Setyan, A., Song, C., Merkel, M., Knighton, W. B., Onasch, T. B., Canagaratna, M. R., Worsnop, D. R., Wiedensohler, A., Shilling, J. E., and Zhang, Q.: Chemistry of new particle growth in mixed urban and biogenic emissions – insights from CARES, *Atmos. Chem. Phys.*, 14, 6477–6494, doi:10.5194/acp-14-6477-2014, 2014.

Shilling, J. E., Zaveri, R. A., Fast, J. D., Kleinman, L., Alexander, M. L., Canagaratna, M. R., Fortner, E., Hubbe, J. M., Jayne, J. T., Sedlacek, A., Setyan, A., Springston, S., Worsnop, D. R., and Zhang, Q.: Enhanced SOA formation from mixed anthropogenic and biogenic emissions during the CARES campaign, *Atmos. Chem. Phys.*, 13, 2091–2113, doi:10.5194/acp-13-2091-2013, 2013.

Titos, G., Jefferson, A., Sheridan, P. J., Andrews, E., Lyamani, H., Alados-Arboledas, L., and Ogren, J. A.: Aerosol light-scattering enhancement due to water uptake during the TCAP campaign, *Atmos. Chem. Phys.*, 14, 7031–7043, doi:10.5194/acp-14-7031-2014, 2014.

Zaveri, R. A., Barnard, J. C., Easter, R. C., Riemer, N., and West, M.: Particle-resolved simulation of aerosol size, composition, mixing state, and the associated optical and cloud condensation nuclei activation properties in an evolving urban plume, *J. Geophys. Res.-Atmos.*, 115, doi:10.1029/2009jd013616, 2010.

Zaveri, R. A., Shaw, W. J., Cziczo, D. J., Schmid, B., Ferrare, R. A., Alexander, M. L., Alexandrov, M., Alvarez, R. J., Arnott, W. P., Atkinson, D. B., Baidar, S., Banta, R. M., Barnard, J. C., Beranek, J., Berg, L. K., Brechtel, F., Brewer, W. A., Cahill, J. F., Cairns, B., Cappa, C. D., Chand, D., China, S., Comstock, J. M., Dubey, M. K., Easter, R. C., Erickson, M. H., Fast, J. D., Floerchinger, C., Flowers, B. A., Fortner, E., Gaffney, J. S., Gilles, M. K., Gorkowski, K., Gustafson, W. I., Gyawali, M., Hair, J., Hardesty, R. M., Harworth, J. W., Herndon, S., Hiranuma, N., Hostetler, C., Hubbe, J. M., Jayne, J. T., Jeong, H., Jobson, B. T., Kassianov, E. I., Kleinman, L. I., Kluzek, C., Knighton, B., Kolesar, K. R., Kuang, C., Kubátová, A., Langford, A. O., Laskin, A., Laulainen, N., Marchbanks, R. D., Mazzoleni, C.,

**Aerosol  
hygroscopicity  
measurements  
during CARES 2010**

D. B. Atkinson et al.

Title Page

Abstract

Introduction

Conclusions

References

Tables

Figures



Back

Close

Full Screen / Esc

Printer-friendly Version

Interactive Discussion



Mei, F., Moffet, R. C., Nelson, D., Obland, M. D., Oetjen, H., Onasch, T. B., Ortega, I., Ottaviani, M., Pekour, M., Prather, K. A., Radney, J. G., Rogers, R. R., Sandberg, S. P., Sedlacek, A., Senff, C. J., Senum, G., Setyan, A., Shilling, J. E., Shrivastava, M., Song, C., Springston, S. R., Subramanian, R., Suski, K., Tomlinson, J., Volkamer, R., Wallace, H. W., Wang, J., Weickmann, A. M., Worsnop, D. R., Yu, X.-Y., Zelenyuk, A., and Zhang, Q.: Overview of the 2010 Carbonaceous Aerosols and Radiative Effects Study (CARES), *Atmos. Chem. Phys.*, 12, 7647–7687, doi:10.5194/acp-12-7647-2012, 2012.

Zelenyuk, A., Yang, J., Choi, E., and Imre, D.: SPLAT II: An aircraft compatible, ultra-sensitive, high precision instrument for in-situ characterization of the size and composition of fine and ultrafine particles, *Aerosol Sci. Tech.*, 43, 411–424, doi:10.1080/02786820802709243, 2009.

Zhang, Q., Jimenez, J. L., Canagaratna, M. R., Ulbrich, I. M., Ng, N. L., Worsnop, D. R., and Sun, Y. L.: Understanding atmospheric organic aerosols via factor analysis of aerosol mass spectrometry: a review, *Anal. Bioanal. Chem.*, 401, 3045–3067, doi:10.1007/s00216-011-5355-y, 2011.

Zhang, X., Massoli, P., Quinn, P. K., Bates, T. S., and Cappa, C. D.: Hygroscopic growth of submicron and supermicron aerosols in the marine boundary layer, *J. Geophys. Res.-Atmos.*, 119, 8384–8399, doi:10.1002/2013JD021213, 2014.

Zieger, P., Fierz-Schmidhauser, R., Gysel, M., Ström, J., Henne, S., Yttri, K. E., Baltensperger, U., and Weingartner, E.: Effects of relative humidity on aerosol light scattering in the Arctic, *Atmos. Chem. Phys.*, 10, 3875–3890, doi:10.5194/acp-10-3875-2010, 2010.

Zieger, P., Fierz-Schmidhauser, R., Weingartner, E., and Baltensperger, U.: Effects of relative humidity on aerosol light scattering: results from different European sites, *Atmos. Chem. Phys.*, 13, 10609–10631, doi:10.5194/acp-13-10609-2013, 2013.

## Aerosol hygroscopicity measurements during CARES 2010

D. B. Atkinson et al.

Title Page

Abstract

Introduction

Conclusions

References

Tables

Figures

◀

▶

◀

▶

Back

Close

Full Screen / Esc

Printer-friendly Version

Interactive Discussion



**Table 1.** Species properties used in model calculations.

PM Component	Real RI	Density (g cm <sup>-3</sup> )	$\kappa$	GF (85 %)
(NH <sub>4</sub> ) <sub>2</sub> SO <sub>4</sub>	1.52	1.77	0.67	1.68
NH <sub>4</sub> NO <sub>3</sub>	1.5	1.73	0.67	1.67
BC	1.9	1.8	0	1.00
Chloride	1.55	2.17	1.2	1.97
HOA	1.45	1	0.006	1.02
OOA	1.49	1.4	<sup>a</sup>	<sup>a</sup>
Supermicron <sup>b</sup>	1.7	2.1	<sup>a</sup>	<sup>a</sup>
Water	1.33	1.0	n/a	n/a

<sup>a</sup> Adjustable.

<sup>b</sup> Technically,  $D_{p,m} > 737$  nm.

## Aerosol hygroscopicity measurements during CARES 2010

D. B. Atkinson et al.

**Table 2.** Change in absolute model retrieved  $\kappa_{\text{OOA}}$  or  $\kappa_{\text{super}}$  for a given perturbation in the assumed hygroscopicities for other particle components ( $\kappa_{\text{other}}$ ), along with sensitivities shown as  $\Delta\kappa_{\text{OOA}}/\Delta\kappa_{\text{other}}$  and  $\Delta\kappa_{\text{super}}/\Delta\kappa_{\text{other}}$ .

Component	$\Delta\kappa_{\text{other}}$ (% and absolute)	T0				T1			
		$\Delta\kappa_{\text{OOA}}$	$\frac{\Delta\kappa_{\text{OOA}}}{\Delta\kappa_{\text{other}}}$	$\Delta\kappa_{\text{super}}$	$\frac{\Delta\kappa_{\text{super}}}{\Delta\kappa_{\text{other}}}$	$\Delta\kappa_{\text{OOA}}$	$\frac{\Delta\kappa_{\text{OOA}}}{\Delta\kappa_{\text{other}}}$	$\Delta\kappa_{\text{super}}$	$\frac{\Delta\kappa_{\text{super}}}{\Delta\kappa_{\text{other}}}$
$(\text{NH}_4)_2\text{SO}_4$	−10% (−0.067)	0.0077	−0.12	0.0077	−0.12	0.0023	−0.034	0.192	−2.86
	+10% (+0.067)	−0.0075	−0.11	−0.0091	−0.14	−0.0070	−0.104	−0.069	−1.03
$\text{NH}_4\text{NO}_3$	−10% (−0.067)	0.0044	−0.065	0.0011	−0.016	0.0014	−0.024	0.0061	−0.091
	+10% (0.067)	−0.0044	−0.065	−0.0014	−0.021	−0.0018		−0.0053	−0.079
BC	n/a (0.02)	−0.0015	−0.075	0.0007	0.035	−0.0004	−0.021	−0.0019	−0.095
	n/a (0.05)	−0.0038	−0.076	0.0021	0.042	0.00045	0.009	−0.0135	−0.27
Chloride	−10% (−0.12)	0.0004	−0.003	0.0005	−0.004	$-6 \times 10^{-6}$	$-5 \times 10^{-5}$	−0.0003	−0.0025
	+7% (0.08)	0.0004	0.005	−0.0005	−0.006	−0.0002	−0.0025	−0.0011	0.0137
HOA	+200% (0.02)	−0.0052	−0.260	$-3 \times 10^{-6}$	−0.0002				
	+733% (0.05)	−0.0167	−0.334	−0.0001	−0.002				
HOA	+67% (0.01)					−0.0004	−0.040	−0.0017	−0.170
	+367% (0.028)					−0.0018	−0.064	−0.0032	−0.114

[Title Page](#)
[Abstract](#)
[Introduction](#)
[Conclusions](#)
[References](#)
[Tables](#)
[Figures](#)
[Back](#)
[Close](#)
[Full Screen / Esc](#)
[Printer-friendly Version](#)
[Interactive Discussion](#)

## Aerosol hygroscopicity measurements during CARES 2010

D. B. Atkinson et al.

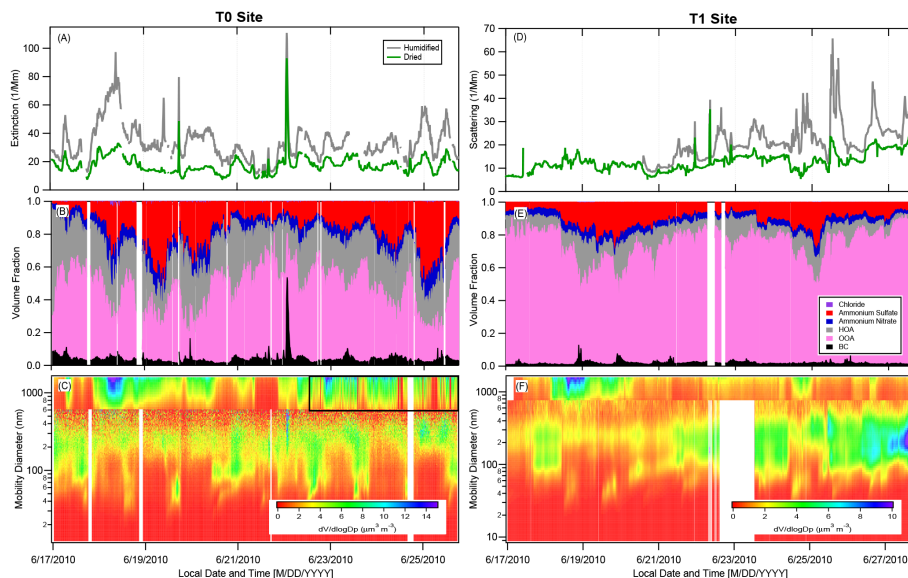


**Figure 1.** Overview time-series data of  $b_{\text{ext}}$  at T0 (left panels) and  $b_{\text{scat}}$  at T1 (right panels) for both humidified and dried particles (**a** and **d**), volume fraction of the various submicron components, exclusive of water (**b** and **e**), and composite volume-weighted size distributions (**c** and **f**). Note that neither the vertical nor the horizontal scales are the same between the two sites/sets of panels. The black box around the last portion of the large particle size distribution at T0 (**c**) indicates the time period during which a synthetic size distribution was used, as described in the text.

Title Page

Abstract

Introduction

Conclusions

References

Tables

Figures



Back

Close

Full Screen / Esc

Printer-friendly Version

Interactive Discussion



## Aerosol hygroscopicity measurements during CARES 2010

D. B. Atkinson et al.

Title Page

Abstract

Introduction

Conclusions

References

Tables

Figures



Back

Close

Full Screen / Esc

Printer-friendly Version

Interactive Discussion

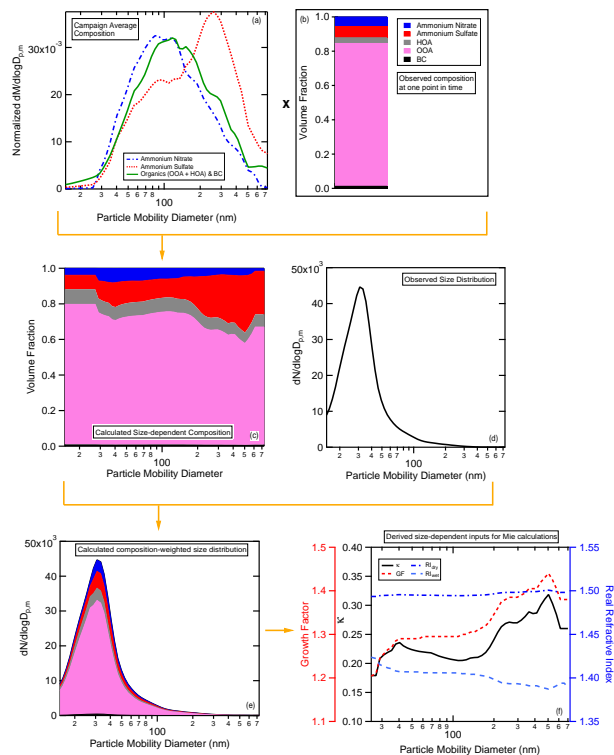


**Figure 2.** Schematic of the process for determining size-dependent hygroscopic growth factors and real refractive indices. The top panels (**a** and **b**) illustrate how the observed campaign-average size-dependent normalized particle composition and the time-dependent particle composition are combined to yield the time- and size-dependent particle composition (**c**). The resulting size-dependent particle composition is combined with the time-dependent size distribution (**d**) to yield a time-dependent size distribution with size-dependent composition (**e**). The resulting size distribution is then used to determine size-dependent growth factors,  $\kappa$  values and real refractive indices (**f**).

## Aerosol hygroscopicity measurements during CARES 2010

D. B. Atkinson et al.

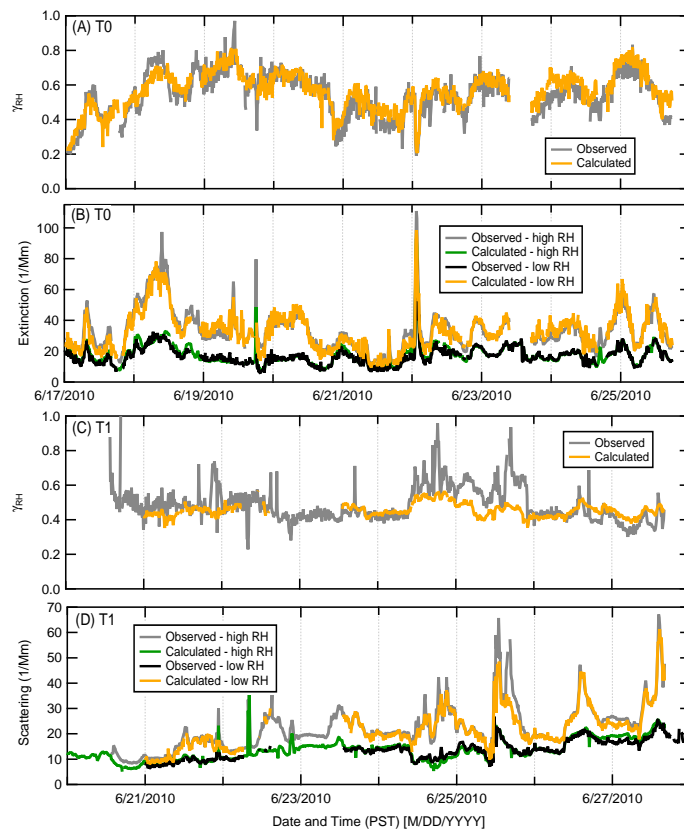


**Figure 3.** Observed and calculated time-series of the lowest (green and black, respectively) and highest (grey and gold, respectively) RH channels for the CRD at T0 **(b)** and humidograph at T1 **(d)**. The observed and calculated optical hygroscopicity parameters ( $\gamma_{RH}$ ) for the two sites are shown as grey and orange, respectively, **(a)** and **(c)**. The calculated traces are produced by the optical hygroscopicity model described in the main text. The vertical line in panel **(b)** denotes the time at which the APS at T0 malfunctioned.

Title Page

Abstract

Introduction

Conclusions

References

Tables

Figures



Back

Close

Full Screen / Esc

Printer-friendly Version

Interactive Discussion



## Aerosol hygroscopicity measurements during CARES 2010

D. B. Atkinson et al.

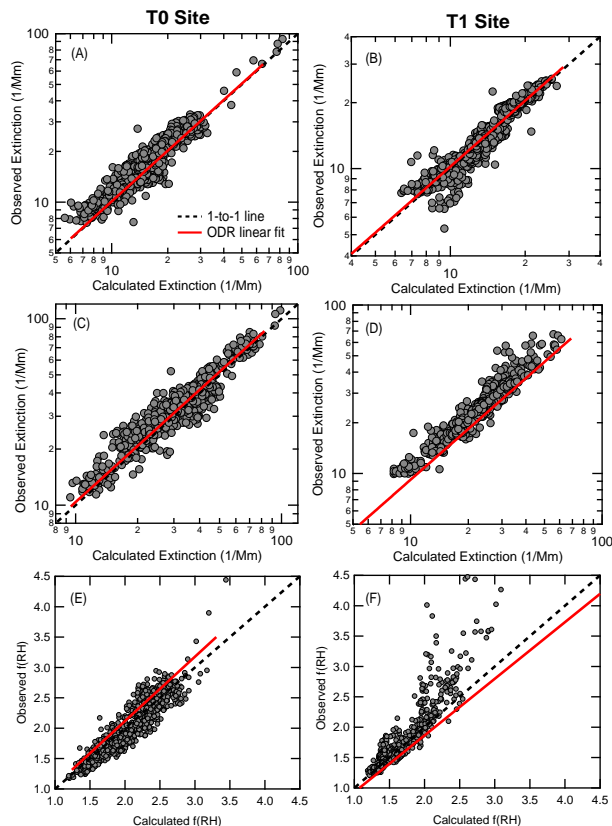


**Figure 4.** Scatterplot comparisons between observed and calculated  $b_{\text{ext}}$  or  $b_{\text{scat}}$  for low RH (**a** and **b**) and high RH (**c** and **d**) and  $f(\text{RH})$  (**e** and **f**) values at the T0 site (left panels) and the T1 site (right panels). The red and dashed lines represent the best ODR linear fit to the data and the 1 : 1 line, respectively. For T0, calculated  $b_{\text{ext, low}}$  and  $b_{\text{ext, high}}$  values are excluded during the period over which synthetic supermicron size distributions were used.

Title Page

Abstract

Introduction

Conclusions

References

Tables

Figures

◀

▶

◀

▶

Back

Close

Full Screen / Esc

Printer-friendly Version

Interactive Discussion





## Aerosol hygroscopicity measurements during CARES 2010

D. B. Atkinson et al.

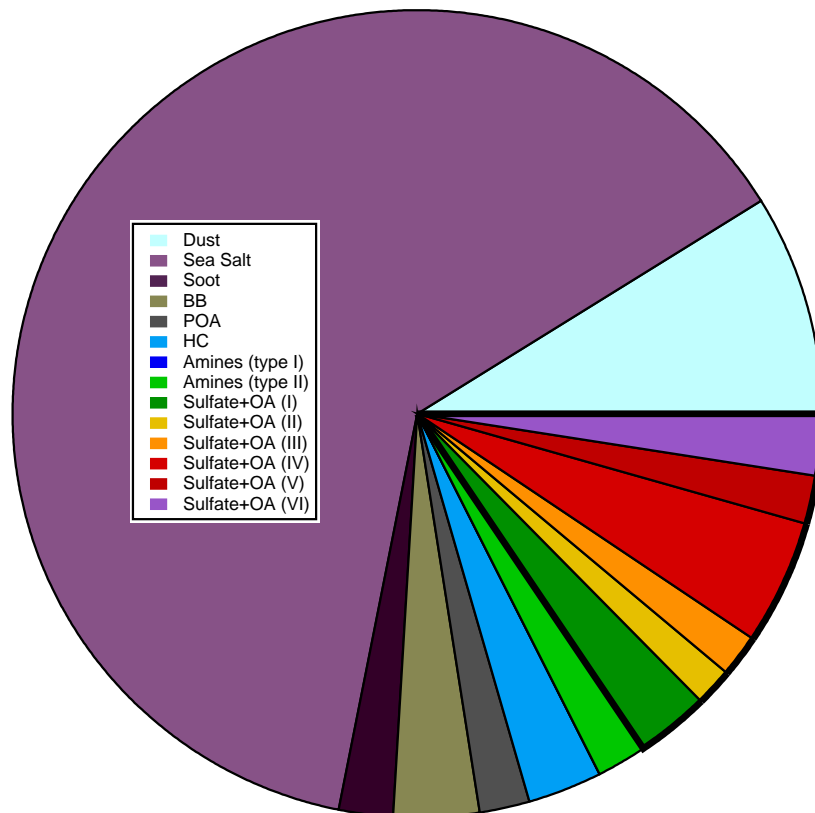


**Figure 6.** Fraction of total sampled number of supermicron particles at T0, as identified by the SPLAT II instrument, over the period 17 June–25 June. It should be noted that the sea salt particle type, which is the most abundant particle type observed, includes particles with varying amounts of NaCl, NaNO<sub>3</sub>, and organics. The solid black outline groups the various Sulfate + OA particle types. (Amine Type I particles were not observed in sufficient abundance to be seen in the pie chart.)

[Title Page](#)
[Abstract](#)
[Introduction](#)
[Conclusions](#)
[References](#)
[Tables](#)
[Figures](#)
[◀](#)
[▶](#)
[◀](#)
[▶](#)
[Back](#)
[Close](#)
[Full Screen / Esc](#)
[Printer-friendly Version](#)
[Interactive Discussion](#)


Aerosol  
hygroscopicity  
measurements  
during CARES 2010

D. B. Atkinson et al.

Title Page

Abstract

Introduction

Conclusions

References

Tables

Figures



Back

Close

Full Screen / Esc

Printer-friendly Version

Interactive Discussion

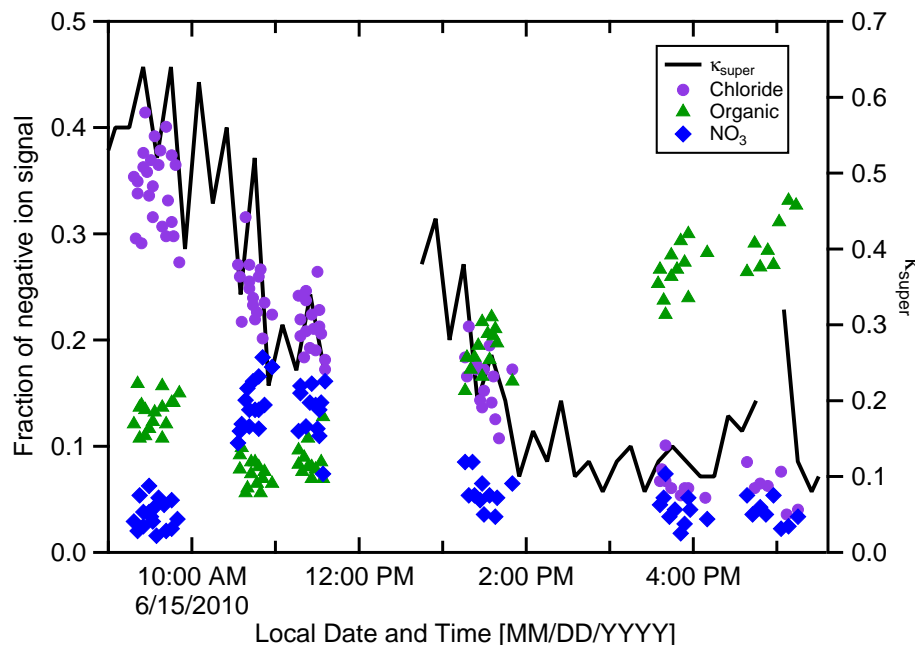


**Figure 7.** Fractional contributions (left axis) of chloride (purple), organics (green) and nitrates (blue) in the PALMS single particle negative ion mass spectra for sea salt-containing particles, identified by sodium in the positive ion spectra, and (right axis) the derived supermicron hygroscopicity parameter,  $K_{\text{super}}$ . The ion fractions do not add up to unity due to contributions from other ion peaks not included here.